H_∞-LQR-Based Coordinated Control for Large Coal-Fired Boiler–Turbine Generation Units

Le Wei, *Member, IEEE*, and Fang Fang, *Member, IEEE*

***Abstract*—The coordinated control system of a boiler–turbine unit plays an important role in maintaining the balance of energy supply and demand, optimizing operational efficiency, and reducing pollutant emissions of the coal-fired power generation unit. The existing challenges (the fast response to wide-scaled load changes, the matching requirements between a boiler and a turbine, and cooperative operation of a large number of distributed devices) make the design of the coordinated controller for the boiler–turbine unit be a tough task. In this paper, based on a typical coal-fired power unit model, using the linear-quadratic regulator (LQR), a coordinated control scheme with H_∞ performance is proposed: the H_∞ method is used to ensure control performance on the basis of reasonable scheduling of distributed equipment; the LQR is applied to limit the control actions to meet the actuator saturation constraints. Case studies for a practical 500 MW coal-fired boiler–turbine unit model indicate that the designed control system has satisfactory performance in a wide operation range and has a very good boiler–turbine coordination capacity.**

***Index Terms*—Boiler–turbine unit, coordinated control, H_∞ performance, linear-quadratic regulator (LQR), saturation constraint.**

I. Introduction

With the growth of energy consumption and the improvements of environmental protection efforts, promoting the application of renewable energy has become an inevitable trend in the world. Over the years, China has been actively optimizing the electric energy structure. As of the end of April 2016, China's installed capacity of 6 megawatts (MW) and above power plants is 1.5 terawatts (TW), where thermal power is of 1.01 TW and grid-connected wind power is of 0.13 TW [1]. In both newly and cumulative installed capacities, China's wind power generation leads the world.

Manuscript received May 28, 2016; revised September 2, 2016; accepted October 3, 2016. Date of publication October 27, 2016; date of current version May 10, 2017. This work was supported in part by the National Natural Science Foundation of China under Grant 51676068 and in part by the Fundamental Research Funds for the Central Universities under Grant 2016MS143 and Grant 2015ZZD15. *(Corresponding author: Fang Fang.)*

L. Wei is with the Control and Computer Engineering School, North China Electric Power University, Baoding 071003, China (e-mail: weile@ncepu.edu.cn).

F. Fang is with the Control and Computer Engineering School, North China Electric Power University, Beijing 102206, China (e-mail: ffang@ncepu.edu.cn).

Color versions of one or more of the figures in this paper are available online at http://ieeexplore.ieee.org.

Digital Object Identifier 10.1109/TIE.2016.2622233

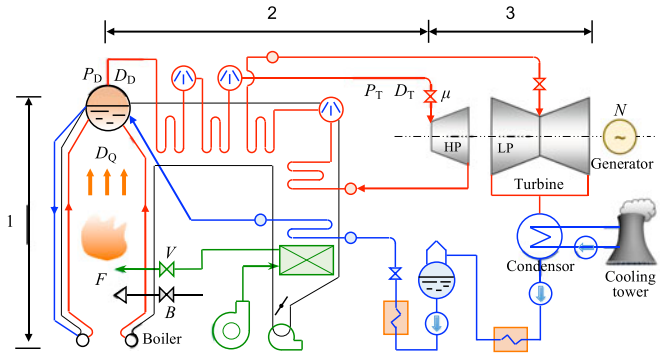

Fig. 1. Schematic diagram of a coal-fired boiler–turbine unit.

TABLE I
NOMENCLATURE OF THE COAL-FIRED BOILER–TURBINE UNIT

Parameter	Description
1	Combustion and heat transfer process in furnace
2	Pipe transfer process
3	Turbine working process
HP	High-pressure cylinder of turbine
LP	Low-pressure cylinder of turbine
B	Boiler firing rate (%)
V	Total air flow entering the furnace (%)
F	Boiler combustion intensity (%)
D_Q	Total effective heat absorption of the boiler (%)
D_D	Steam flow through the pipes (%)
P_D	Drum pressure (MPa)
D_T	Steam flow entering the turbine (%)
P_T	Throttle pressure (MPa)
μ	Throttle valve position (%)
N	Megawatt output (MW)

However, the randomness and the fluctuation of the renewable energy power (wind power, solar power, etc.) have adverse influence on the stability of power grid and the electric power quality. Therefore, to improve the level of control and operation of back-up and schedulable power supply has been one of the most important issues for large-capacity renewable energy access. For China, by taking into account that coal-fired thermal power occupies an overwhelming superiority, increasing the operation flexibility (raising the load change rate and reducing the minimum stable load) of coal-fired power generation becomes an inevitable and effective choice.

A boiler–turbine unit is the most efficient and economical form of the coal-fired power generation, as shown in Fig. 1 [2] (its corresponding parameters are described in Table I).

It is a huge distributed system.

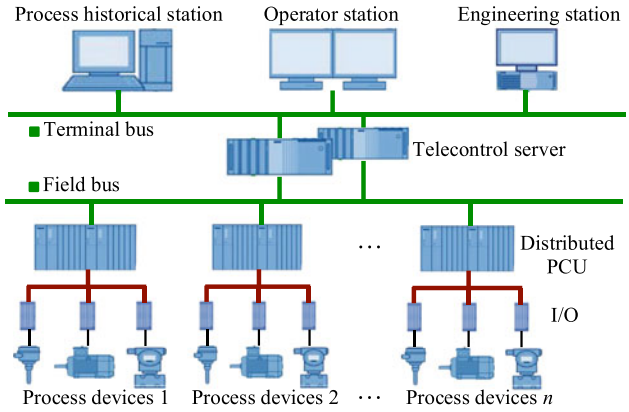

Fig. 2. System configuration for a distributed control system of a boiler–turbine unit.

1) There are thousands of operating devices in the power generation process. These devices are distributed in a broad space (workshop volume of 7×10^5 m^3, plant area of 8×10^5 m^2).
2) There are nearly ten thousand input/output (I/O) measuring points (large ultrasupercritical units will have much more measuring points).
3) There are 500–600 separate control loops that automatically operate their corresponding devices according to their intended targets in order to ensure the normal operation of each device.

In order to undertake a large number of measurement and control tasks, and to reduce the operational risk of such a huge modern production process, distributed control systems (DCSs) are employed in almost all of the power plants in China. The DCS is an industrial computer system with a complex network structure. It consists of functionally and/or geographically distributed digital process control units (PCUs) capable of executing from regulatory control loops. The PCUs are usually designed redundantly to enhance the reliability of the control system. The system configuration of a typical DCS for a boiler–turbine unit is shown in Fig. 2. This is in contrast to a nondistributed system, which uses a single controller at a central location. Corresponding to the production processes, all of the separate control loops of the boiler–turbine unit are classified into several subcontrol systems. One PCU manages one or more subcontrol systems. And all PCUs are connected by communication networks for command and monitoring.

However, each subcontrol system does not exist independently. They have to work coordinately for a goal (making the power output of the boiler–turbine unit meet the load demand from the power grid with a favourable flexibility). To achieve this goal, only relying on the hardware platform of the DCS is not enough, a coordinated control strategy is much-needed.

The tasks of the coordinated control strategy should include three aspects:

1) the coordination between the energy demand of power-grid users and the power output of the boiler–turbine unit (power-grid-level energy supply and demand balance);
2) the coordination between the thermal energy output of the boiler side and the energy demand of the turbine side (boiler–turbine-unit-level energy supply and demand balance);
3) the coordination between the related equipment of each production link and the basic control loops (device-level coordinated operation).

But, for a coal-fired boiler–turbine unit, the above-mentioned three coordinations are not easy to achieve. The reasons are

1) Coal composition is not stable (coal composition differs greatly for different coal mines).
2) The dynamic characteristics of the boiler and the steam turbine are very different.
3) The user power demand from the power grid is random.

Therefore, in order to ensure that such a huge distributed energy conversion system can provide power to users safely, steadily, efficiently, and flexibly, setting up a coordinated control system (CCS) for the boiler–turbine unit is imperative.

1) From the aspect of a power grid, a CCS is a link between the power grid and the boiler–turbine unit, and is the boiler–turbine-unit-side executor of automatic generation control [3], [4];
2) From the aspect of the boiler–turbine unit, a CCS is a coordinator of the operation-characteristics difference between the boiler and the turbine;
3) From the aspect of local control loops, a CCS is a conductor of coordinating each equipment with subcontrol loops.

Fig. 3 shows the hierarchical control structure of a boiler–turbine unit, where the subcontrol systems are at the process control level and the CCS is at the process monitoring level. From the relationship between the CCS and the subcontrol systems of the boiler–turbine unit, we know the following.

1) It is a complicated control system with hierarchical and distributed structure;
2) The measuring points involved in each local control systems and the actuators are distributed in each part of the boiler–turbine unit;
3) The coordination control is at the top level and belongs to the category of supervisory and control;
4) The control outputs of the CCS controllers are the target instructions of the boiler-side and the turbine-side basic control loops.

For a boiler–turbine unit, such a large-scale DCS (which has received many researchers attention [5], [6]), the fast response to the load is coupled with the stability maintenance of main operating parameters. So one goal of the boiler–turbine CCS is to solve the coupling problem [7]. Some PID-form decoupling controllers were deduced for industrial applications [8]. But the presence of uncertain disturbances will affect the decoupling effect; therefore, robust control [9], [10], predictive control [11]–[13], and fuzzy control [14] have been introduced. Noticing that the static and dynamic characteristics of a boiler–turbine unit change gradually with the load change and time pass, some methods have been adopted for the wide working conditions, e.g., gain-scheduled control [15], data-driven control [16], nonlinear dynamics and control of bifurcation [17], adaptive backstepping control [2], [18], and generic nonsmooth H_∞ output synthesis [19]. However, the practical applicability of these methods and the actuator saturation constraints, which

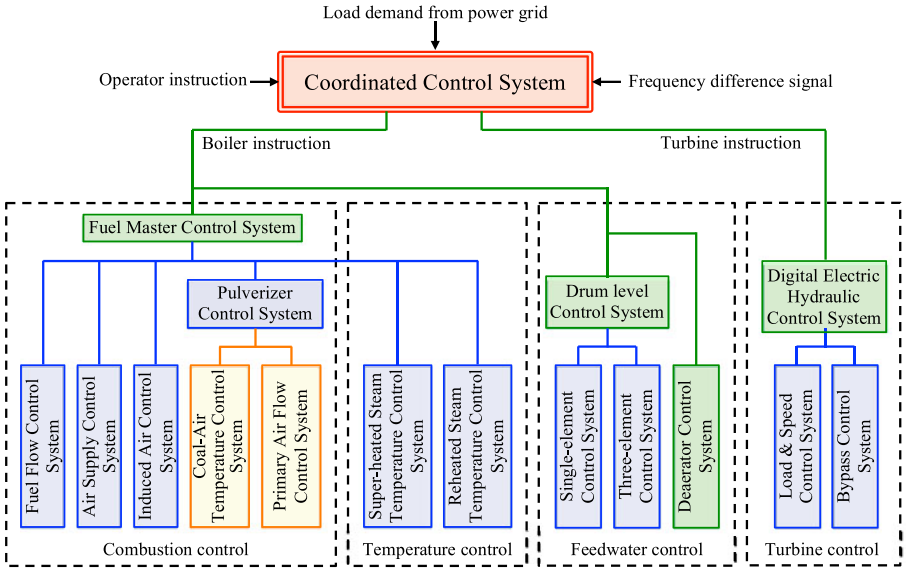

Fig. 3. Hierarchical control structure of a boiler–turbine unit.

gets more and more attention of researchers [20], were not fully considered.

In this paper, taking into account the engineering application requirements (simple control structure, stable, antidisturbance, robust, and meeting the actuator saturation constraints), by using the linear-quadratic regulator (LQR), a coordinated control scheme with H_∞ performance is proposed: the H_∞ method is used to synthesize controllers achieving stabilization with guaranteed performance [21]; the LQR is applied to limit the control actions to meet the actuator saturation constraints. The proposed approach makes the following contributions and advantages to conventional H_∞ methods.

1) The distributed control loops can respond and cooperate with each other better.
2) The system outputs can accurately track their demands.
3) The control actions are relatively smooth, and can meet the actuator saturation nonlinear constraints.
4) Better tracking performance or more smooth control inputs can be obtained by modifying the weight factors during the controller design procedure.
5) The proposed H_∞-LQR-based CCS controller is simple in structure and easy to be implemented in the DCS.

The rest of the paper is arranged as follows: in Section II, the coal-fired boiler–turbine units is modeled, and the problem is formulated; Section III gives the design procedure of the H_∞-LQR-based coordinated control scheme; in Section IV, a practical nonlinear model of a 500 MW coal-fired boiler–turbine unit is used to test the efficiency of the proposed control system; conclusion remarks are made in Section V.

II. Boiler–Turbine Unit Modeling and Problem Formulation

A. Model of the Boiler–Turbine Unit

The energy conversion and transfer process of a coal-fired boiler–turbine unit, shown in Fig. 1, can be divided into three processes:

1) Combustion and Heat Transfer Process in Furnace: By using Δ to represent increment, this process can be described as

$$\Delta D_Q(s) = \frac{k_1}{(T_1 s+1)(T_2 s+1)}\Delta B(s). \tag{1}$$

2) Pipe Transfer Process: When we treat the boiler and the main steam pipes as a concentrate thermal storage container, the pipe transfer process can be described as

$$\Delta D_Q(t) - \Delta D_T(t) = c\frac{d\Delta P_D(t)}{dt}, \tag{2}$$

$$P_D(t) - P_T(t) = k_T D_T^2(t) \tag{3}$$

and

$$D_T(t) = k_T \mu(t) P_T(t). \tag{4}$$

3) Turbine Working Process: For a turbine with reheater, the dynamic transfer function of its working process is

$$N(s) = \frac{(\alpha T_3 s+1)k_2}{T_3 s+1} D_T(s). \tag{5}$$

The coefficients in (1)–(5) are described in Table II. And the dynamic diagram of the three processes is shown in Fig. 4. This is the so-called Cheres model [22], a well-known simplified nonlinear model for boiler–turbine units. It has been tested by Cheres in five different capacity units, and has been widely recognized and applied in control system analyses and design for more than 20 years.

Remark 1: (*Necessity of choosing the simplified model*) For the boiler–turbine unit, such a complicated and distributed system, if precise modeling is carried out for each local production process, the overall mathematical model of the boiler–turbine unit will have the feature of distributed parameter and very high model order. This kind of model is suitable for simulation and verification, but will be disastrous for the model-based control system design.

TABLE II
NOMENCLATURE OF FIG. 4

Parameter	Description
α	Proportion of the megawatt output of HP in the total megawatt output (MW/MW)
c	Thermal storage constant of the boiler and the main steam pipes (%/MPa)
k_1	Gain of the combustion process in the furnace (%/%)
k_2	Gain of the turbine (MPa/%)
k_μ	Gain of the relationship between P_T, μ, and D_T (%/(%· MPa))
k_T	Resistance constant of the steam pipes and the throttle valve (MPa/%^{2})
T_1	Inertia time of the combustion process in the furnace (s)
T_2	Inertia time of the heat transfer process in the furnace (s)
T_3	Inertia time constant of the turbine (s)

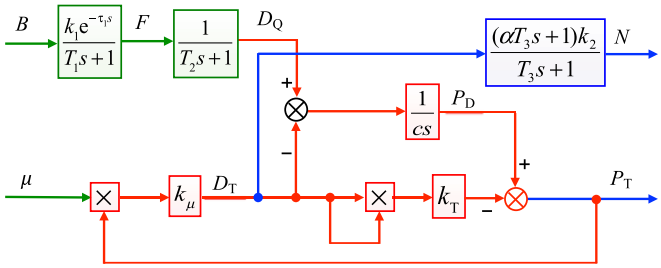

Fig. 4. Dynamic diagram of the Cheres model.

Remark 2: (Feasibility of choosing the simplified model) Although the Cheres model chosen in this paper is simple, it can accurately describe the energy exchange process and the energy balance of the boiler–turbine unit, and can reflect the effect of the control signals (B and μ) on the unit power outputs. All of these are the contents concerned by the CCS at the process monitoring level. So the choice of this model is appropriate and applicable for the CCS design.

B. Problem Formulation

From the overall system perspective, the coal-fired boiler–turbine unit is a 2×2 nonlinear multivariable system. The two inputs are B and μ, and the two outputs are N and P_T. Furthermore, there exist actuator saturation nonlinear constraints in the control signals to be implemented B and μ, which can be expressed as $0\% \le B \le 100\%$ and $0\% \le \mu \le 100\%$. These constraints must be taken into account when designing the controller.

So, a CCS controller should be designed to coordinate all the distributed equipment by generating reasonable instructions B and μ. The control objectives of the CCS are ensuring N fast track its demand N_r in a wide operation range, while keeping P_T accurately following its set-point P_{Tr}.

III. CONTROL SYSTEM DESIGN

A. Model Preprocessing

In this part, we will preprocess the typical coal-fired boiler–turbine model to a suitable form for the controller design.

Following the design procedure of the classic H_∞ approach, we can design a controller to fulfill the first four requirements. But in order to design the controller by means of the linear matrix inequalities (LMIs) approach, we should first linearize the Cheres model.

Suppose that the system is working at an equilibrium condition $[\mu_0, B_0, P_{T0}, N_0, P_{D0}, D_{Q0}, D_{T0}]$ and the deviation around the equilibrium point is small enough. Then, we rewrite (3) and (4) in incremental form, and get

$$\Delta P_D(t) - \Delta P_T(t) = R\Delta D_T(t), \tag{6}$$

$$\Delta D_T(t) = k_\mu \mu_0 \Delta P_T(t) + k_\mu P_{T0} \Delta\mu(t) \tag{7}$$

where $R := 2k_T D_{T0}$ is the steam flow resistance constant (MPa/%).

It is inferred from (2), (6), and (7) that

$$\Delta P_T(s) = \frac{1}{k_\mu \mu_0 (T_0 s+1)} \Delta D_Q(s) - \frac{P_{T0}(T_b s+1)}{\mu_0 (T_0 s+1)} \Delta\mu(s) \tag{8}$$

$$\Delta D_T(s) = \frac{1}{T_0 s+1} \Delta D_Q(s) + \frac{k_\mu P_{T0} T_t s}{T_0 s+1} \Delta\mu(s). \tag{9}$$

Here, the time constants (s) are defined as

$$T_0 = \left(R + \frac{1}{k_\mu \mu_0}\right) c, T_b = Rc, T_t = \frac{c}{k_\mu \mu_0}, T_0 = T_b + T_t \tag{10}$$

where T_0 will be different under different working conditions.

Because the inertia T_2 is relatively small, the relation between B and D_Q, shown in Fig. 4, can be further simplified as

$$\Delta D_Q(s) = \frac{k_1}{T_1 s+1} \Delta B(s). \tag{11}$$

Following Fig. 4 and (8)–(11), the nonlinear system has been linearized as

$$\begin{bmatrix} \Delta P_T(s) \\ \Delta N(s) \end{bmatrix} = \boldsymbol{G}_T(s) \boldsymbol{G}_0(s) \boldsymbol{G}_F(s) \begin{bmatrix} \Delta B(s) \\ \Delta\mu(s) \end{bmatrix} \tag{12}$$

with

1) dynamic processes of the turbine

$$\boldsymbol{G}_T(s) = \begin{bmatrix} 1 & 0 \\ 0 & \dfrac{k_2(\alpha T_3 s+1)}{T_3 s+1} \end{bmatrix} \tag{13}$$

2) dynamic processes of the fuel

$$\boldsymbol{G}_F(s) = \begin{bmatrix} \dfrac{k_1}{T_1 s+1} & 0 \\ 0 & 1 \end{bmatrix} \tag{14}$$

3) dynamic processes of the boiler

$$\boldsymbol{G}_0(s) = \begin{bmatrix} \dfrac{1}{k_\mu \mu_0 (T_0 s+1)} & -\dfrac{P_{T0}(T_b s+1)}{\mu_0 (T_0 s+1)} \\ \dfrac{1}{T_0 s+1} & \dfrac{k_\mu P_{T0} T_t s}{T_0 s+1} \end{bmatrix}. \tag{15}$$

Certainly, we can design an H_∞ controller for the whole linearized model, but this will lead to a rather complicated control

law. From (13)–(15), we can see that the coupling and the uncertainty of the model only exist in $\boldsymbol{G}_0(s)$, so we can first choose D_Q and μ as assistant inputs to design a controller for this part, then get the final controller according to the relationship between this part and the whole system.

Then, the first task is to decouple $\boldsymbol{G}_0(s)$. Although this is not necessary, it makes the impact of the design parameters on the system performance clearer without increasing the system complexity.

Letting $\tilde{\boldsymbol{G}}_0(s)$ be the expected transfer function matrix of the decoupled part and $\boldsymbol{G}'(s)$ be the transfer function matrix of decoupling device, we have

$$\tilde{\boldsymbol{G}}_0(s) = \boldsymbol{G}_0(s)\boldsymbol{G}'(s). \tag{16}$$

In order to facilitate the controller design, we take $\tilde{\boldsymbol{G}}_0(s)$ as a diagonal matrix. And under the condition that the pole positions are not changed, the main diagonal elements are simplified in the typical first-order inertial form

$$\tilde{\boldsymbol{G}}_0(s) = \begin{bmatrix} \dfrac{1}{k_\mu \mu_0 (T_0 s+1)} & 0 \\ 0 & \dfrac{1}{T_0 s+1} \end{bmatrix}. \tag{17}$$

Then, from (15)–(17), we can obtain

$$\boldsymbol{G}'(s) = \begin{bmatrix} \dfrac{T_t s}{T_0 s+1} & \dfrac{T_b s+1}{T_0 s+1} \\ -\dfrac{1}{k_\mu P_{T0}(T_0 s+1)} & \dfrac{1}{k_\mu P_{T0}(T_0 s+1)} \end{bmatrix}. \tag{18}$$

Furthermore, for the existence of the dynamic processes of the fuel (14), we add its inversion $\boldsymbol{G}_F^{-1}(s)$ in the decoupling device in order to use D_Q and μ as the assistant inputs. Then, the final decoupler is

$$\begin{aligned} \boldsymbol{G}^*(s) = \boldsymbol{G}_F^{-1}(s)\boldsymbol{G}'(s) &= \begin{bmatrix} \dfrac{T_1 s+1}{k_1} & 0 \\ 0 & 1 \end{bmatrix} \\ &\times \begin{bmatrix} \dfrac{T_t s}{T_0 s+1} & \dfrac{T_b s+1}{T_0 s+1} \\ -\dfrac{1}{k_\mu P_{T0}(T_0 s+1)} & \dfrac{1}{k_\mu P_{T0}(T_0 s+1)} \end{bmatrix} \\ &= \begin{bmatrix} \dfrac{T_t s(T_1 s+1)}{k_1(T_0 s+1)} & \dfrac{(T_b s+1)(T_1 s+1)}{k_1(T_0 s+1)} \\ -\dfrac{1}{k_\mu P_{T0}(T_0 s+1)} & \dfrac{1}{k_\mu P_{T0}(T_0 s+1)} \end{bmatrix}. \end{aligned} \tag{19}$$

Suppose that the assistant input vector is the input vector of the decoupling device $\boldsymbol{u}(t) = [\Delta B(t), \Delta\mu(t)]^T$, the assistant output vector is

$$\boldsymbol{y}(t) = \begin{bmatrix} \Delta P_T(t) \\ \Delta D_T(t) \end{bmatrix} = \begin{bmatrix} P_T(t) - P_{T0} \\ D_T(t) - D_{T0} \end{bmatrix} \tag{20}$$

and the state vector is $\boldsymbol{x}(t) = \boldsymbol{y}(t)$, then the decoupled part can be expressed in the state-space form as follows:

$$\begin{aligned} \dot{\boldsymbol{x}}(t) &= \boldsymbol{A}\boldsymbol{x}(t) + \boldsymbol{B}\boldsymbol{u}(t) \\ \boldsymbol{y}(t) &= \boldsymbol{C}\boldsymbol{x}(t) \end{aligned} \tag{21}$$

where the matrices $\boldsymbol{A}$, $\boldsymbol{B}$, $\boldsymbol{C}$ are

$$\boldsymbol{A} = -\frac{1}{T_0}\boldsymbol{I}_{2\times 2}, \boldsymbol{B} = \operatorname{diag}\left(\frac{1}{\mu_0 T_0}, \frac{1}{T_0}\right), \boldsymbol{C} = \boldsymbol{I}_{2\times 2}.$$

B. State Vector Expansion

In this part, by introducing the integral of the system tracking errors, the state vector of the preprocessed model will be expanded to ensure the control system having satisfactory tracking ability.

Noticing that the classic H_∞ approach can only achieve the robust performance and the stabilization of a system, but cannot ensure the system outputs accurately tracking their set-points, we introduce a new vector

$$\boldsymbol{x}_e(t) = \int_0^t [\boldsymbol{y}_r(\tau) - \boldsymbol{y}(\tau)]d\tau \tag{22}$$

with

$$\boldsymbol{y}_r(t) = \begin{bmatrix} \Delta P_{Tr}(t) \\ \Delta D_{Tr}(t) \end{bmatrix} = \begin{bmatrix} P_{Tr}(t) - P_{T0} \\ D_{Tr}(t) - D_{T0} \end{bmatrix} \tag{23}$$

where D_{Tr} is the demand of D_T, to represent the integral of the system tracking errors. Then, the system state vector can be augmented as $\boldsymbol{x}(t) = [\boldsymbol{x}^{\mathrm{T}}(t), \boldsymbol{x}_e^{\mathrm{T}}(t)]^{\mathrm{T}}$.

Let the control signal $\boldsymbol{u}(t)$ be

$$\boldsymbol{u}(t) = \boldsymbol{K}\boldsymbol{X}(t) \tag{24}$$

where $\boldsymbol{K} := [\boldsymbol{K}_p, \boldsymbol{K}_i]$, $\boldsymbol{K}_p \in \boldsymbol{R}^{2\times 2}$, and $\boldsymbol{K}_i \in \boldsymbol{R}^{2\times 2}$. Then, the controller is a generalized PI controller. Now, the augmented closed-loop system can be expressed as

$$\dot{\boldsymbol{X}}(t) = (\bar{\boldsymbol{A}} + \bar{\boldsymbol{B}}_1\boldsymbol{K})\boldsymbol{X}(t) + \bar{\boldsymbol{B}}_2\boldsymbol{y}_r(t), \tag{25}$$

$$\boldsymbol{y}(t) = \begin{bmatrix} \boldsymbol{C} & 0_{2\times 2} \end{bmatrix} \boldsymbol{X}(t) \tag{26}$$

with

$$\bar{\boldsymbol{A}} = \begin{bmatrix} \boldsymbol{A} & 0_{2\times 2} \\ -\boldsymbol{C} & 0_{2\times 2} \end{bmatrix}, \bar{\boldsymbol{B}}_1 = \begin{bmatrix} \boldsymbol{B}_1 \\ -\boldsymbol{D} \end{bmatrix}, \bar{\boldsymbol{B}}_2 = \begin{bmatrix} 0_{2\times 2} \\ \boldsymbol{I}_{2\times 2} \end{bmatrix}.$$

C. Objective Function Construction

Here, we will construct the comprehensive control performance cost function with the expanded state vector and the control action vector to meet the actuator saturation constraints.

Since the H_∞ approach cannot be directly applied to deal with the hard actuator constraints, we include the magnitude of the control actions in the comprehensive control performance cost function, which is the main idea of the LQR.

To ensure the system stability and tracking ability, and to constrain the control actions, the cost function is chosen as

$$\begin{aligned} J = \int_0^\infty \{&[\boldsymbol{x}_e^{\mathrm{T}}(t)\boldsymbol{Q}\boldsymbol{x}_e(t) + \boldsymbol{u}^{\mathrm{T}}(t)\boldsymbol{R}\boldsymbol{u}(t)] \\ &-\gamma^2 \boldsymbol{Y}_r^{\mathrm{T}}(t)\boldsymbol{Y}_r(t) + \dot{V}(t)\}\mathrm{d}t \end{aligned} \tag{27}$$

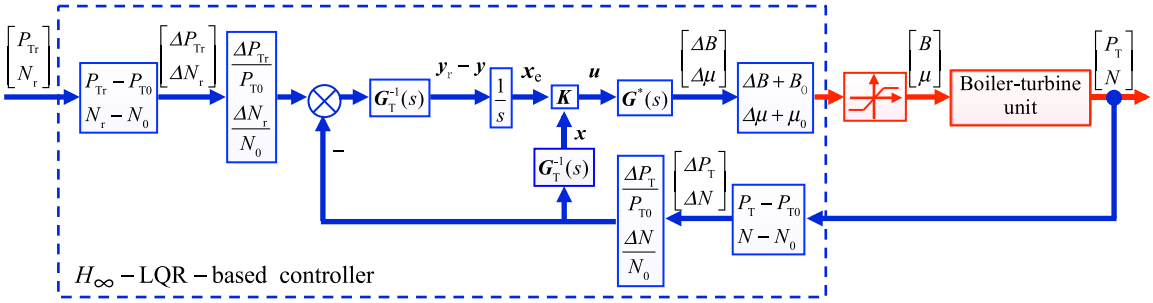

Fig. 5. Dynamic diagram of the H_∞-LQR-based control system for the boiler–turbine unit.

where weighting factors $\boldsymbol{Q} \in \boldsymbol{R}^{2\times 2}$ and $\boldsymbol{R} \in \boldsymbol{R}^{2\times 2}$ are given positive definite symmetric matrices, and $V(t)$ is a Lyapunov functional candidating for the system in (25) as follows:

$$V(t) = \boldsymbol{X}^{\mathrm{T}}(t)\boldsymbol{P}\boldsymbol{X}(t). \tag{28}$$

Here, $\boldsymbol{P}$ is a positive defined symmetric matrix.

Suppose the controlled output vector is chosen as

$$\boldsymbol{Z}(t) = \boldsymbol{x}_e^{\mathrm{T}}(t)\boldsymbol{Q}\boldsymbol{x}_e(t) + \boldsymbol{u}^{\mathrm{T}}(t)\boldsymbol{R}\boldsymbol{u}(t) \tag{29}$$

and letting

$$\boldsymbol{Q}_1 = \begin{bmatrix} 0_{2\times 2} & \sqrt{\boldsymbol{Q}} \\ 0_{2\times 2} & 0_{2\times 2} \end{bmatrix}, \boldsymbol{R}_1 = \begin{bmatrix} 0_{2\times 2} \\ \sqrt{\boldsymbol{R}} \end{bmatrix}, \boldsymbol{E} = \boldsymbol{Q}_1 + \boldsymbol{R}_1\boldsymbol{K} \tag{30}$$

we obtain

$$\boldsymbol{Z}(t) = \boldsymbol{Q}_1\boldsymbol{X}(t) + \boldsymbol{R}_1\boldsymbol{u}(t) = \boldsymbol{E}\boldsymbol{X}(t). \tag{31}$$

Then, the objective function can be rewritten as

$$J = \int_0^\infty [\boldsymbol{Z}^{\mathrm{T}}(t)\boldsymbol{Z}(t) - \gamma^2\boldsymbol{Y}_r^{\mathrm{T}}(t)\boldsymbol{Y}_r(t) + \dot{V}(t)]\mathrm{d}t. \tag{32}$$

Thus, the problem of the generalized PI controller design is converted into a problem of the state-feedback control for the augmented system. The control goal is to find a desired controller $\boldsymbol{u}(t) = \boldsymbol{K}\boldsymbol{X}(t)$ such that the closed-loop system in (25) and (31) is asymptotically stable and the objective function in (32) satisfies $J < 0$.

Definition 1: Given a positive scalar γ, the closed-loop control system in (25) and (31) is said to be asymptotically stable with a prescribed H_∞ performance γ, if it is asymptotically stable and

$$\|\boldsymbol{Z}(t)\|_2^2 < \gamma^2\|\boldsymbol{Y}_r(t)\|_2^2 \tag{33}$$

for all nonzero $\boldsymbol{Y}_r(t) \in l_2[0,\infty)$ subject to the zero initial condition, where $\|\boldsymbol{Z}(t)\|_2^2 = \int_0^\infty \boldsymbol{Z}^{\mathrm{T}}(t)\boldsymbol{Z}(t)\mathrm{d}t$ and $\|\boldsymbol{Y}_r(t)\|_2^2 = \int_0^\infty \boldsymbol{Y}_r^{\mathrm{T}}(t)\boldsymbol{Y}_r(t)\mathrm{d}t$.

Remark 3: From (32) and $J < 0$, we obtain

$$J = \|\boldsymbol{Z}(t)\|_2^2 - \gamma^2\|\boldsymbol{Y}_r(t)\|_2^2 + V(\boldsymbol{X}(\infty)) - V(\boldsymbol{X}(0)) < 0. \tag{34}$$

Noticing that $V(\boldsymbol{X}(0)) = 0$ and $V(\boldsymbol{X}(\infty)) \geq 0$, we can conclude that

$$\|\boldsymbol{Z}(t)\|_2^2 < \gamma^2\|\boldsymbol{Y}_r(t)\|_2^2. \tag{35}$$

So, we can say that this is an H_∞-LQR-based problem. According to Fig. 4, (20), (23), and (24), we get the dynamic diagram of the H_∞-LQR-based control system for boiler–turbine units as shown in Fig. 5.

D. Problem Conversion

Now, we will convert the problem of ensuing the cost function be negative to the LMIs problem, and deduce the H_∞-LQR-based coordinated control law by solving the LMIs problem.

To convert the H_∞-LQR-based control problem to the LMIs problem, the following theorems are needed.

Theorem 1: For given γ, $\boldsymbol{K}$, $\boldsymbol{Q}$, and $\boldsymbol{R}$, the closed-loop system in (25) and (31) is asymptotically stable and the performance index in (32) satisfies $J < 0$, if there exists a positive defined symmetric matrix $\boldsymbol{P}$ satisfying

$$\begin{bmatrix} \boldsymbol{\Phi}_1 & \boldsymbol{P}\bar{\boldsymbol{B}}_2 \\ \bar{\boldsymbol{B}}_2^{\mathrm{T}}\boldsymbol{P} & -\gamma^2\boldsymbol{I} \end{bmatrix} < 0 \tag{36}$$

where

$$\boldsymbol{\Phi}_1 = \boldsymbol{Q}_1^{\mathrm{T}}\boldsymbol{Q}_1 + \boldsymbol{K}^{\mathrm{T}}\mathbf{R}\mathbf{K} + \bar{\boldsymbol{A}}^{\mathrm{T}}\boldsymbol{P} + \boldsymbol{P}\bar{\boldsymbol{A}} + \boldsymbol{K}^{\mathrm{T}}\bar{\boldsymbol{B}}_1^{\mathrm{T}}\boldsymbol{P} + \boldsymbol{P}\bar{\boldsymbol{B}}_1\boldsymbol{K}. \tag{37}$$

Proof 1: For the unforced system of (25), the derivative of the Lyapunov function can be evaluated as

$$\begin{aligned}\dot{V}(t) &= \frac{\partial \boldsymbol{X}^{\mathrm{T}}(t)}{\partial t}\boldsymbol{P}\boldsymbol{X}(t) + \boldsymbol{X}^{\mathrm{T}}(t)\boldsymbol{P}\frac{\partial \boldsymbol{X}(t)}{\partial t} \\ &= \boldsymbol{X}^{\mathrm{T}}(t)(\bar{\boldsymbol{A}}^{\mathrm{T}}\boldsymbol{P} + \boldsymbol{P}\bar{\boldsymbol{A}} + \boldsymbol{K}^{\mathrm{T}}\bar{\boldsymbol{B}}_1^{\mathrm{T}}\boldsymbol{P} + \boldsymbol{P}\bar{\boldsymbol{B}}_1\boldsymbol{K})\boldsymbol{X}(t).\end{aligned} \tag{38}$$

From (36) and (37), we have

$$\boldsymbol{Q}_1^{\mathrm{T}}\boldsymbol{Q}_1 + \boldsymbol{K}^{\mathrm{T}}\boldsymbol{R}\boldsymbol{K} + \bar{\boldsymbol{A}}^{\mathrm{T}}\boldsymbol{P} + \boldsymbol{P}\bar{\boldsymbol{A}} + \boldsymbol{K}^{\mathrm{T}}\bar{\boldsymbol{B}}_1^{\mathrm{T}}\boldsymbol{P} + \boldsymbol{P}\bar{\boldsymbol{B}}_1\boldsymbol{K} < 0. \tag{39}$$

For $\boldsymbol{R} = \boldsymbol{R}^{\mathrm{T}} \geq 0$, we obtain

$$\bar{\boldsymbol{A}}^{\mathrm{T}}\boldsymbol{P} + \boldsymbol{P}\bar{\boldsymbol{A}} + \boldsymbol{K}^{\mathrm{T}}\bar{\boldsymbol{B}}_1^{\mathrm{T}}\boldsymbol{P} + \boldsymbol{P}\bar{\boldsymbol{B}}_1\boldsymbol{K} < 0. \tag{40}$$

From (38) and (40), we know that $\dot{V}(t) < 0$. Then, according to the Lyapunov theory, the closed-loop system in (25) and (31) is asymptotically stable.

Next, from (36), we know that

$$\begin{bmatrix} \boldsymbol{X}^{\mathrm{T}}(t) & \boldsymbol{Y}_r^{\mathrm{T}}(t) \end{bmatrix} \begin{bmatrix} \boldsymbol{\Phi} & \boldsymbol{P}\bar{\boldsymbol{B}}_2 \\ \bar{\boldsymbol{B}}_2^{\mathrm{T}}\boldsymbol{P} & -\gamma^2\boldsymbol{I} \end{bmatrix} \begin{bmatrix} \boldsymbol{X}(t) \\ \boldsymbol{Y}_r(t) \end{bmatrix} < 0 \tag{41}$$

that is,

$$[\boldsymbol{x}_e^{\mathrm{T}}(t)\boldsymbol{Q}\boldsymbol{x}_e(t)+\boldsymbol{u}^{\mathrm{T}}(t)\boldsymbol{R}\boldsymbol{u}(t)]-\gamma^2\boldsymbol{Y}_r^{\mathrm{T}}(t)\boldsymbol{Y}_r(t)+\dot{V}(t)<0. \tag{42}$$

From (27) and (42), we have $J<0$. ■

Theorem 2: Consider the closed-loop system in (25) and (31). For given $\boldsymbol{Q}$ and $\boldsymbol{R}$, if and only if there exist matrices $\boldsymbol{P}_1>0$ and $\boldsymbol{M}$ with appropriate dimensions and $\xi>0$ such that the LMI in (43) holds

$$\begin{bmatrix}[\bar{\boldsymbol{A}}\boldsymbol{P}_1]_s+[\bar{\boldsymbol{B}}_1\boldsymbol{M}]_s & \bar{\boldsymbol{B}}_2 & \boldsymbol{P}_1\boldsymbol{Q}_1^{\mathrm{T}} & \boldsymbol{M}^{\mathrm{T}}\\ \bar{\boldsymbol{B}}_2^{\mathrm{T}} & -\xi\boldsymbol{I} & 0 & 0\\ \boldsymbol{Q}_1\boldsymbol{P}_1 & 0 & -\boldsymbol{I} & 0\\ \boldsymbol{M} & 0 & 0 & -\boldsymbol{R}^{-1}\end{bmatrix}<0. \tag{43}$$

Then, there exists a proper controller $\boldsymbol{u}(t)=\boldsymbol{K}\boldsymbol{X}(t)$ such that the closed-loop system is asymptotically stable with an H_∞ attenuate level $\gamma=\sqrt{\xi}$ and (36) are satisfied with $\boldsymbol{P}=\boldsymbol{P}_1^{-1}$ and the desired state feedback control gain matrix is

$$\boldsymbol{K}=\boldsymbol{M}\boldsymbol{P}_1^{-1}. \tag{44}$$

Proof 2: Take $\boldsymbol{P}=\boldsymbol{P}_1^{-1}$, $\boldsymbol{K}=\boldsymbol{M}\boldsymbol{P}_1^{-1}$, and $\gamma=\sqrt{\xi}$ into (43), then left and right multiply the result by the matrix

$$\boldsymbol{P}_2=\begin{bmatrix}\boldsymbol{P}_1^{-1} & 0 & 0 & 0\\ 0 & \boldsymbol{I} & 0 & 0\\ 0 & 0 & \boldsymbol{I} & 0\\ 0 & 0 & 0 & \boldsymbol{I}\end{bmatrix} \tag{45}$$

we obtain

$$\begin{bmatrix}\boldsymbol{\Phi}_2 & \boldsymbol{P}\bar{\boldsymbol{B}}_2 & \boldsymbol{Q}_1^{\mathrm{T}} & \boldsymbol{K}^{\mathrm{T}}\\ \bar{\boldsymbol{B}}_2^{\mathrm{T}}\boldsymbol{P} & -\gamma^2\boldsymbol{I} & 0 & 0\\ \boldsymbol{Q}_1 & 0 & -\boldsymbol{I} & 0\\ \boldsymbol{K} & 0 & 0 & -\boldsymbol{R}^{-1}\end{bmatrix}<0 \tag{46}$$

where

$$\boldsymbol{\Phi}_2=\boldsymbol{K}^{\mathrm{T}}\bar{\boldsymbol{B}}_1^{\mathrm{T}}\boldsymbol{P}+\bar{\boldsymbol{A}}^{\mathrm{T}}\boldsymbol{P}+\boldsymbol{P}\bar{\boldsymbol{A}}+\boldsymbol{P}\bar{\boldsymbol{B}}_1\boldsymbol{K}. \tag{47}$$

Then, by using Schur complement, (46) yields condition (36). ■

Then, by solving the LMI problem (43), we can obtain the state feedback control gain matrix $\boldsymbol{K}$ from (44). Then, according to Fig. 5, we finally get the H_∞-LQR-based control system for boiler–turbine units.

IV. Case Studies

In order to test the performance of the proposed controller, a practical 500 MW nonlinear boiler–turbine model of Shen-tou $2^{\#}$ power plant in Shan-xi, China [2], as shown in Fig. 4, is used in this section. The initial model inputs are [$B_0=100\%$, $\mu_0=100\%$], the limits of both control actions are [0%, 100%], and the initial states are [$P_{D0}=18.97$ MPa, $P_{T0}=16.18$ MPa, $D_{Q0}=100\%$, $N_0=500$ MW]. The model coefficients, which are obtained from practical operating data, are $\alpha=0.25$ MW/MW, $c=6.489\%$/MPa, $k_1=1\%/\%$, $k_2=500$ MW/%, $k_\mu=0.0618\%/(\%\cdot\text{MPa})$, $k_T=2.3116$ MPa/(%^{2}), $T_1=150$ s, $T_2=6$ s, $T_3=6$ s.

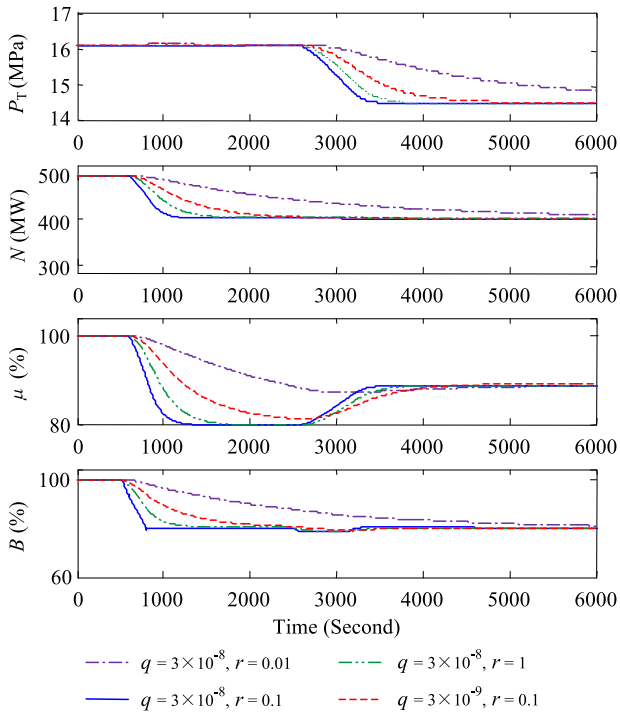

Fig. 6. Time responses with different values of q and r.

To design the controller, we linearize the model and obtain the corresponding per-unit values of the coefficients in (13)–(15) as $T_0=135$ s, $T_b=30$ s, $T_t=105$ s, $P_{T0}=100\%$, $N_0=100\%$, $\mu_0=100\%$, $k_1=1\%/\%$, $k_2=1\%/\%$, $T_3=6$ s, and $T_1=150$ s.

The weighting factor matrices $\boldsymbol{Q}$ and $\boldsymbol{R}$ in (27) are determined by the trail method. To be simple, we suppose $\boldsymbol{Q}=\mathrm{diag}(q,q)$ and $\boldsymbol{R}=\mathrm{diag}(r,r)$, where q and r are the weighting factors to be determined. Fig. 6 shows the system responses with different values of q and r, when N_r step decreases from 500 to 400 MW at $t=500$ s and P_{Tr} step decreases from 16.18 to 14.562 MPa at $t=2500$ s.

From Fig. 6, we can see that the time responses with $q=3\times10^{-8}, r=0.1$ are the fastest. With this set of weighting factors, and by solving (43) and (44), we obtain the gain matrix $\boldsymbol{K}$ as

$$\boldsymbol{K}=\begin{bmatrix}-3.1220 & 0 & 0.0231 & 0\\ 0 & -3.1315 & 0 & 0.0232\end{bmatrix}. \tag{48}$$

To compare the control performance, a classic PI decoupling control system is adopted, whose block diagram is shown in Fig. 7, where the decoupler $\boldsymbol{D}(s)$ is

$$\boldsymbol{D}(s)=[\boldsymbol{G}_T(s)\boldsymbol{G}_0(s)\boldsymbol{G}_F(s)]^{-1}\cdot\boldsymbol{G}_{\mathrm{dc}}(s). \tag{49}$$

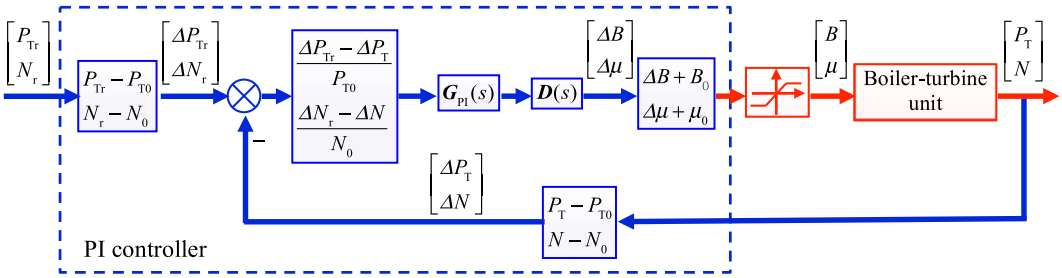

Fig. 7. Block diagram of the classic PI decoupling control system for the boiler–turbine unit.

From (12)–(15), we obtain

$$\boldsymbol{G}_T(s)\boldsymbol{G}_0(s)\boldsymbol{G}_F(s) = \begin{bmatrix} \dfrac{k_1}{k_\mu\mu_0(T_0s+1)(T_1s+1)} & -\dfrac{P_{T0}(T_b+1)}{\mu_0(T_0s+1)} \\ \dfrac{k_1k_2(\alpha T_3s+1)}{(T_0s+1)(T_3s+1)} & \dfrac{k_2k_\mu P_{T0}T_ts(\alpha T_3s+1)}{(T_0s+1)(T_3s+1)} \end{bmatrix}. \tag{50}$$

Then, desired decoupled transfer function of the plant $\boldsymbol{G}_{\rm dc}(s)$ can be chosen following four requirements.

1) It is a diagonal matrix.
2) The static gain of each control channel is 1.
3) The pole positions are kept unchanged.
4) Each channel has a pure differential or first-order differential link to improve the response speed.

Here, choose $\boldsymbol{G}_{\rm dc}(s)$ as

$$\boldsymbol{G}_{\rm dc}(s) = \begin{bmatrix} \dfrac{k_1s}{\mu_0(T_0s+1)(T_1s+1)} & 0 \\ 0 & \dfrac{P_{T0}k_2(\alpha T_3s+1)}{(T_0s+1)(T_3s+1)} \end{bmatrix} \tag{51}$$

then the decoupler $\boldsymbol{D}(s)$ can be deduced as

$$\boldsymbol{D}(s) = \begin{bmatrix} \dfrac{T_ts}{T_0s+1} & \dfrac{P_{T0}(T_1s+1)(T_bs+1)}{k_1(T_0s+1)(\alpha T_3s+1)} \end{bmatrix}. \tag{52}$$

By fitting $\boldsymbol{G}_{\rm dc}(s)$ to one-order inertia plus delay form, we can get the PI controller according to the Ziegler–Nichols method [23] as

$$\boldsymbol{G}_{\rm PI}(s) = {\rm diag}(3.6 + 0.0216/s, 25.92 + 1.552/s). \tag{53}$$

In the whole design procedure of the PI controller, we notice that the actuator saturation constraints are not considered.

A. Tracking Ability Test

In order to ensure economic operation, the boiler–turbine unit operation mode is more complicated: under high load conditions ($N_r > 375$ MW), P_{Tr} is maintained constant while the load demand N_r is changing, which is called the constant pressure operation mode (CPOM); under low load conditions, the relationship between N_r and P_{Tr} is denoted by Fig. 8, which is called the sliding pressure operation mode (SPOM).

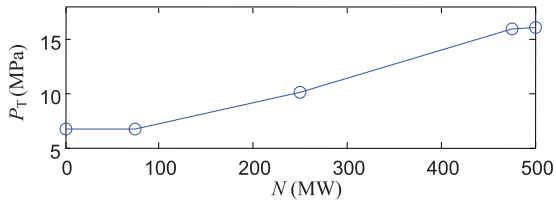

Fig. 8. Sliding pressure curve of the 500 MW boiler–turbine unit.

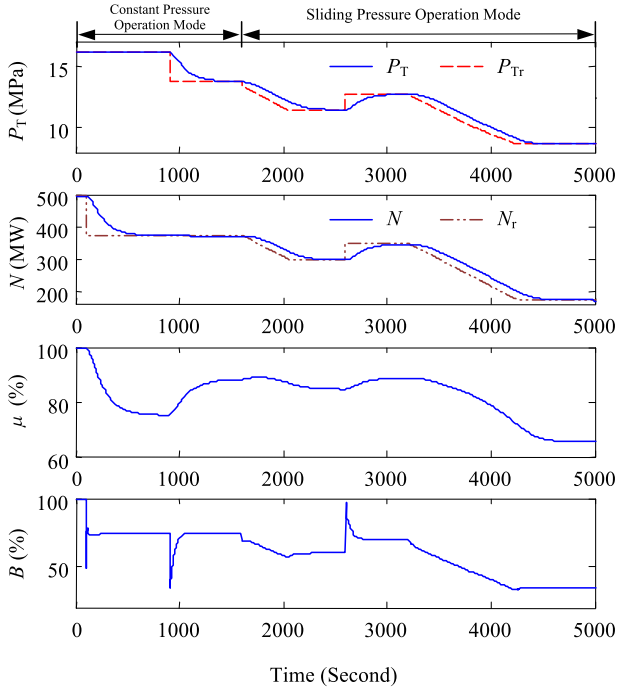

Fig. 9. Responses of the tracking ability test of the H_∞-based LQR control system under both operation modes with the actuator saturation constraints.

The time responses of the proposed H_∞-based LQR control system are shown in Fig. 9. When time is before 4000 s, the system is operating under the CPOM, and later it works under the SPOM.

1) Under the CPOM, N and P_T can accurately follow N_r and P_{Tr}, respectively. The adjustment processes are monotonical and smooth, and the settling times are not more than 500 s. The two control channels are well decoupled.

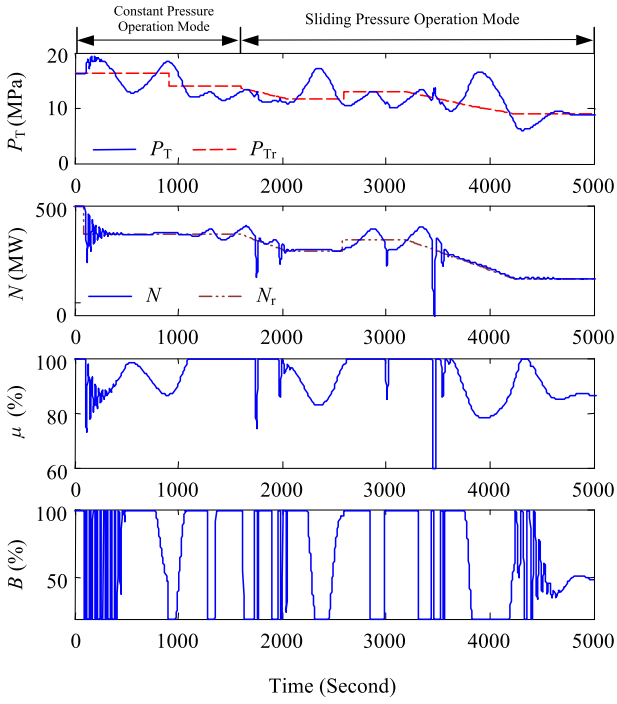

Fig. 10. Responses of the tracking ability test of the PID control system under both operation modes with the actuator saturation constraints.

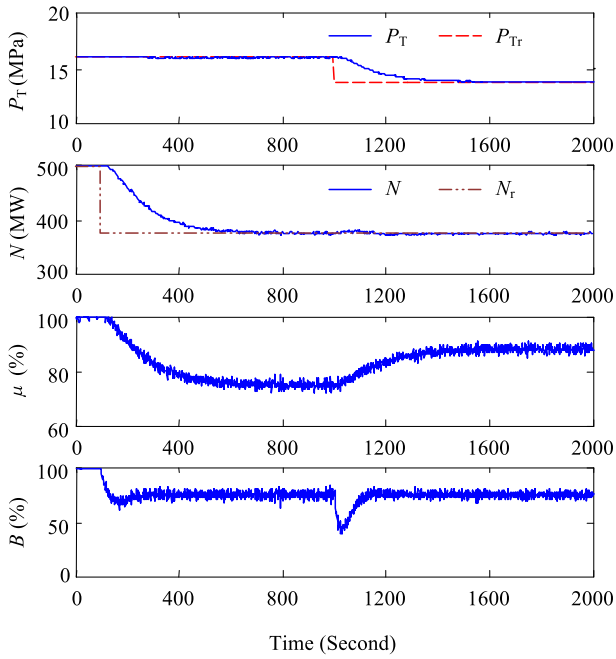

Fig. 11. Responses of the antidisturbance ability test under the constant pressure operation mode.

2) Under the SPOM, N_r and P_{Tr} change (step change or ramp change) at the same time, but N and P_T can still follow them, respectively.
3) In the whole process, the changes of the control signals (governor valve position and boiler firing rate) are reasonable.

For comparison, the output responses and the control actions of the classic PI decoupling control system are shown in Fig. 10. We can see that

1) The adjustment procedures are oscillating and the settling times are much longer.
2) With the actuator saturation nonlinear constraints, the control performance is rather bad.

B. Antidisturbance Ability Test

Considering a boiler–turbine unit often receives high-frequency noise interference in its operation process, we add two zero-mean white noise disturbances with 1% variances into the control signals. The disturbance of μ is added from $t = 0$ s, and the disturbance of B is added from $t = 100$ s. The responses are shown in Fig. 11. We can see that N and P_T fluctuate with the white noise disturbances. But the fluctuations are very small in the amplitude. That is to say, the system has good antidisturbance ability.

C. Parameter Tuning and Application Discussion

In the H_∞-LQR optimal design procedure, after the controlled object model is determined, the controller $\boldsymbol{K}$ is decided only by the state weight matrix $\boldsymbol{Q}$ and the control signal weight matrix $\boldsymbol{R}$, so the choice of $\boldsymbol{Q}$ and $\boldsymbol{R}$ is particularly important. As a diagonal matrix, the greater the elements of $\boldsymbol{Q}$, the higher the state constraints become. And also, the greater the corresponding elements of $\boldsymbol{R}$, the greater the control signal constraints become.

After the normalization of all the state variables, we can reasonably assume that $\boldsymbol{Q} = \mathrm{diag}(q, q)$ and $\boldsymbol{R} = \mathrm{diag}(r, r)$. Then, in the control system design process, only two parameters (q and r) need to be determined, which, comparing with the traditional PID parameter tuning, is much easier.

As shown in Fig. 5, the proposed H_∞-LQR-based controller is a linear controller. Its structure is simple and can be easily realized by the configuration software of the DCS.

V. Conclusion

In this paper, a novel boiler–turbine unit control scheme based on the H_∞-LQR-based control approach was presented for improving load adaptability of power generation units in a wide range of working conditions.

Compared with the existing work, the new features of the proposed controller are as follows.

1) After the state vector expansion, it ensures the system outputs accurately tracking their set-points, which cannot be achieved by the classic H_∞ approach.
2) It combines the approaches H_∞ and LQR together. This means that it can ensure the control quality of the system under the premise of satisfying the control signal constraints.
3) It is a linear controller, its structure is simple and the control actions can meet the actuator saturation constraints.

All of these mean that the proposed controller can be easily achieved in the DCS.

4) The outputs of the coordinated controller are more stable, and it is beneficial to the distributed basic control loops to better respond and cooperate with each other.

However, there are still some features that can be improved in the future.

1) The choice of the weighting factors (q and r) is a key and tedious step in the design procedure of the H_∞-LQR-based controller. It directly affects the performance of the control system. From the application point of view, to promote the engineering applicability of the proposed control scheme, it is necessary to establish a lookup table associating each type/capacity of boiler–turbine unit and its weighting factors' values (or ranges) by means of experiments or simulations.
2) We only study the control problem of boiler–turbine units with actuator saturation in this paper. However, dead zone, quick opening, equal percentage, square root, etc., are also common nonlinear characteristics of actuators, and worth further study, although nonlinear compensation, control performance improvement, stability proof, etc., would be challenging problems.

REFERENCES

[1] China Electricity Council. (2016, May). Brief introduction to the operation of electricity industry from January 2016 to April 2016. [Online]. Available: http://www.cec.org.cn/guihuayutongji/gongxufenxi/dianliyunxingjiankuang/2016-05-18/153080.html

[2] F. Fang and L. Wei, "Backstepping-based nonlinear adaptive control for coal-fired utility boiler-turbine units," *Appl. Energy*, vol. 88, no. 3, pp. 814–824, Mar. 2011.

[3] J. Játiva-Ibarra, M. I. Morales, W. J. Cabrera, F. L. Quilumba, and W. J. Lee, "AGC parameter determination for an oil facility electric system," *IEEE Trans. Ind. Appl.*, vol. 20, no. 4, pp. 2876–2882, Jul./Aug. 2014.

[4] M. Giuntoli and D. Poli, "Optimized thermal and electrical scheduling of a large scale virtual power plant in the presence of energy storages," *IEEE Trans. Smart Grid*, vol. 4, no. 2, pp. 942–955, Mar. 2013.

[5] H. P. Li, W. S. Yan, Y. Shi, and Y. T. Wang, "Periodic event-triggering in distributed receding horizon control of nonlinear systems," *Syst. Control Lett.*, vol. 86, pp. 16–23, Dec. 2015.

[6] M. X. Liu, Y. Shi, and X. T. Liu, "Distributed MPC of aggregated heterogeneous thermostatically controlled loads in smart grid," *IEEE Trans. Ind. Electron.*, vol. 63, no. 2, pp. 1120–1129, Feb. 2016.

[7] H. C. Gery, "The evolution of coordinated control," *Inst. Soc. Amer. Power Symp. Inst. Power Ind.*, vol. 31, pp. 109–112, May 1988.

[8] F. Fang, W. Tan, and J. Z. Liu, "Tuning of coordinated controllers for boiler-turbine units," *Acta Automat. Sinica*, vol. 31, no. 2, pp. 291–296, Mar. 2005.

[9] M. Hamed, B. N. Firooz, and S. A. Majid, "Robust control of an industrial boiler system: A comparison between two approaches: Sliding mode control h_∞ technique," *Energy Convers. Manage.*, vol. 50, no. 6, pp. 1401–1410, Jun. 2009.

[10] L. Batool, J. M. Horacio, and T. W. Chen, "Decentralized robust pi controller design for an industrial boiler," *J. Process Control*, vol. 19, no. 2, pp. 216–230, Feb. 2009.

[11] K. Y. Lee, J. H. V. Sickel, J. A. Hoffman, W. H. Jung, and S. H. Kim, "Controller design for a large-scale ultrasupercritical once-through boiler power plant," *IEEE Trans. Energy Convers.*, vol. 25, no. 4, pp. 1063–1070, Dec. 2010.

[12] G. Prasad, G. W. Irwin, E. Swidenbank, and B. W. Hogg, "Plant-wide predictive control for a thermal power plant based on physical plant model," *Proc. Inst. Elect. Eng.—Control Theory Appl.*, vol. 147, no. 5, pp. 523–537, Sep. 2000.

[13] S. Lu and B. W. Hogg, "Predictive co-ordinated control for power-plant steam pressure and power output," *Control Eng. Pract.*, vol. 5, no. 1, pp. 79–84, Jan. 1997.

[14] A. Abdennour, "An intelligent supervisory system for drum type boilers during severe disturbances," *Int. J. Elect. Power Energy Syst.*, vol. 22, no. 5, pp. 381–387, Jun. 2000.

[15] P. C. Chen and J. S. Shamma, "Gain-scheduled ℓ^1-optimal control for boiler-turbine dynamics with actuator saturation," *J. Process Control*, vol. 14, no. 3, pp. 263–277, Apr. 2004.

[16] F. Fang and Y. Xiong, "Event-driven-based water level control for nuclear steam generators," *IEEE Trans. Ind. Electron.*, vol. 61, no. 10, pp. 5480–5489, Oct. 2014.

[17] H. Moradi, A. Alasty, and G. Vossoughi, "Nonlinear dynamics and control of bifurcation to regulate the performance of a boiler-turbine unit," *Energy Convers. Manage.*, vol. 68, pp. 105–113, Apr. 2013.

[18] Y. S. Wang and X. H. Yu, "New coordinated control design for thermal-power-generation units," *IEEE Trans. Ind. Electron.*, vol. 57, no. 11, pp. 3848–3856, Nov. 2010.

[19] I. U. Ponce, J. Bentsman, Y. Orlov, and L. T. Aguilar, "Generic nonsmooth H_∞ output synthesis: Application to a coal-fired boiler/turbine unit with actuator dead zone," *IEEE Trans. Control Syst. Technol.*, vol. 23, no. 6, pp. 2117–2128, Nov. 2015.

[20] H. P. Li and Y. Shi, "Network-based predictive control for constrained nonlinear systems with two-channel packet dropouts," *IEEE Trans. Ind. Electron.*, vol. 61, no. 3, pp. 1574–1582, Mar. 2014.

[21] H. Zhang, Y. Shi, and M. X. Liu, "H_∞ step tracking control for networked discrete-time nonlinear systems with integral and predictive actions," *IEEE Trans. Ind. Informat.*, vol. 9, no. 1, pp. 337–345, Feb. 2013.

[22] E. Cheres, Z. J. Palmor, and J. Tuch, "Drum type boiler following control configuration," *IEEE Trans. Energy Convers.*, vol. 9, no. 1, pp. 199–205, Mar. 1994.

[23] K. Ogata, *Modern Control Engineering*, 4th ed. Englewood Cliffs, NJ, USA: Prentice-Hall, Nov. 2001.

Le Wei (M'14) received the M.Sc. degree in control theory and engineering and the Ph.D. degree in thermal power engineering from North China Electric Power University, Baoding, China, in 2001 and 2009, respectively.

She is currently an Associate Professor in the School of Control and Computer Engineering, North China Electric Power University, Baoding. Her current research interests include modeling, adaptive control, and optimal control of power generation units.

Fang Fang (M'09) received the M.Sc. degree in control theory and engineering from North China Electric Power University, Baoding, China, in 2001, and the Ph.D. degree in thermal power engineering from North China Electric Power University, Beijing, China, in 2005.

He is currently a Professor in the School of Control and Computer Engineering, North China Electric Power University, Beijing. He has been involved in more than 20 academic research and industrial technology projects. His current research interests include modeling and control of power generation units, optimal configuration and operation of combined cooling, heat, and power systems, and energy management of smart buildings.